arXiv:1701.02197v1 [cond-mat.dis-nn] 9 Jan 2017

Ising Spin Glasses in dimension two; universality and non-universality

P. H. Lundow[1] and I. A. Campbell[2]

[1] *Department of Mathematics and Mathematical Statistics, Umeå University, SE-901 87, Sweden*
[2] *Laboratoire Charles Coulomb, Université Montpellier II, 34095 Montpellier, France*

Following numerous earlier studies, extensive simulations and analyses were made on the continuous interaction distribution Gaussian model and the discrete bimodal interaction distribution Ising Spin Glass (ISG) models in dimension two (P.H. Lundow and I.A. Campbell, Phys. Rev. E **93**, 022119 (2016)). Here we further analyse the bimodal and Gaussian data together with data on two other continuous interaction distribution 2D ISG models, the uniform and the Laplacian models, and three other discrete interaction distribution models, a diluted bimodal model, an "anti-diluted" model, and a more exotic symmetric Poisson model. Comparisons between the three continuous distribution models show that not only do they share the same exponent $\eta \equiv 0$ but that to within the present numerical precision they share the same critical exponent ν also, and so lie in a single universality class. On the other hand the critical exponents of the four discrete distribution models are not the same as those of the continuous distributions, and differ from one discrete distribution model to another. Discrete distribution ISG models in dimension two have non-zero values of the critical exponent η; they do not lie in a single universality class.

PACS numbers: 75.50.Lk, 05.50.+q, 64.60.Cn, 75.40.Cx

I. INTRODUCTION

The canonical dimension $d = 2$ Edwards-Anderson (EA) model Ising spin glasses (ISGs) on square lattices with either Gaussian or bimodal ($\pm J$) nearest neighbor interaction distributions have been the subject of numerous studies over many years. Below we will refer in particular to our own measurements on these two models [1]. There are analytic arguments that these two archetype models (and by extension all 2D ISG models with other distributions) have zero-temperature transitions [2, 3].

After explaining the simulation and analysis techniques used, we first present data on two other continuous distribution models : the uniform and the Laplacian interaction distribution models, comparing with the Gaussian model. For the Gaussian model, where the interaction distribution is continuous and the ground state for each individual sample is unique, there is a general consensus concerning the thermodynamic limit (ThL) critical exponents : $\eta \equiv 0$, $\nu = 3.52(2)$ [4–9]. We find that not only is the anomalous dimension critical exponent $\eta \equiv 0$ for each of these three models as it must be, but also that the correlation length exponent is $\nu = 3.52(5)$ for all three models to within the precision of the present numerical data extrapolations. The data are thus compatible with all 2D continuous interaction distribution models lying in a single universality class.

For the 2D bimodal model the interaction distribution is discrete and the ground state is highly degenerate. There are two limiting regimes, with a size dependent crossover temperature $T^*(L)$ [10], a $T < T^*(L)$ ground state plus gap dominated regime and an effectively continuous energy level regime $T > T^*(L)$. There have been consistent estimates over decades from correlation function measurements [11, 12], Monte Carlo renormalization-group measurements [13], transfer matrix calculations [14], numerical simulations [1, 15–17], and ground state measurements [18, 19] showing that the anomalous dimension critical exponent $\eta \approx 0.20$ in both regimes, indicating that the bimodal model is not in the same universality class as the continuous distribution models. However, it has also been claimed that the bimodal model in the $T > T^*(L)$ regime is in the same universality class as the Gaussian model, because for the bimodal model : "fits... lead to values of η that are very small, between 0 and 0.1, strongly suggestive of $\eta = 0$" [10], and "the data are not sufficiently precise to provide a precise determination of η, being consistent with a small value $\eta \leq 0.2$, including $\eta = 0$" [20, 21]. Recently the much more definitive statement has been made : "we can safely summarize our findings as $|\eta| < 0.02$." [9].

We discuss the Binder cumulant/correlation length ratio comparison approach [22] in the 2D context, as applied to the continuous interaction distribution models and to the bimodal model, and then the Quotient approach used in Ref. [9] as applied to the bimodal model. From both approaches we deduce estimates for the bimodal ISG exponents in the $T > T^*(L)$ regime which are fully compatible with our previous conclusions Ref. [1] including $\eta \approx 0.20$.

We then study three other discrete interaction distribution models : a diluted bimodal ISG, an "anti-diluted" bimodal model and a symmetric Poisson model. Using the approach of Ref. [1] and the correlation length ratio/Binder cumulant approach we conclude that each discrete interaction model has a non-zero anomalous dimension exponent η and lies in an individual universality class.

II. SIMULATIONS AND ANALYSIS

Simulations were carried out on square lattice Ising spin glasses (ISGs) with near neighbor interactions, up to size $L = 128$ and with $N = 2^{13} = 8192$ independent samples at each size. Each of the 2D ISG models orders only at zero temperature. As in Ref. [1] where measurements were made on the square lattice ISG models with Gaussian and bimodal interaction distributions, the samples were equilibrated using the Houdayer method [15] with four replicas; all the simulation techniques are identical to those already described in detail in Ref. [1]. As far as could be judged by reading off the figures shown in Ref. [9], all the raw Gaussian and bimodal data in the [9] and [1] simulation sets are in full agreement with each other to within the statistics. For the present data analysis, in addition to using T as the temperature scaling variable, which is a standard convention for models which order at zero temperature, we use $\tau_b = 1/(1+\beta^2)$, where $\beta = 1/T$, as the scaling variable (see Ref. [1]). This variable is appropriate for ISGs with $T_c = 0$ because of the symmetry between positive and negative interactions in the distributions, and because τ_b has the limits $\tau_b = 0$ at $T = 0$, and $\tau_b = 1$ at infinite temperature and so is well adapted to the Wegner scaling approach [23]. For consistency, when using this scaling variable we scale not the bare second moment correlation length $\xi(\tau_b, L)$ but the normalized correlation length $\xi(\tau_b, L)/\beta$ following a general rule for ISGs in any dimension [24]. The normalized correlation length (like the susceptibility $\chi(\tau_b, L)$ and the normalized Binder cumulant $g(\tau_b, L)L^2$), tends to 1 and not to 0 at infinite temperature; in consequence the behavior of $\xi(\tau_b, L)/\beta$ over the entire temperature range can be expressed to good precision using only a few finite Wegner correction terms.

For any distribution, for samples of size L in the temperature range where $L \gtrsim 7\xi(\tau_b, L)$ all observables are practically independent of L and so can be considered to be in the Thermodynamic limit (ThL) regime where observable values at finite L are equal to the infinite size limit values. This regime can be readily identified by inspection of scaling plots.

In order to underline the validity of the analysis procedure which was used for the bimodal and Gaussian ISG data in Ref. [1] and which is again used below for the other ISG models, in Appendix I we apply the same procedure to the Fully Frustrated (FF) Villain model, a well understood 2D Ising model with a strongly degenerate ground state which has a zero temperature ferromagnetic ordering point and known critical behavior.

III. THE 2D CONTINUOUS DISTRIBUTION ISG MODELS

The standard ISG Hamiltonian is $\mathcal{H} = -\sum_{ij} J_{ij} S_i S_j$ with the near neighbor symmetric distributions normalized to $\langle J_{ij}^2 \rangle = 1$. The normalized inverse temperature is

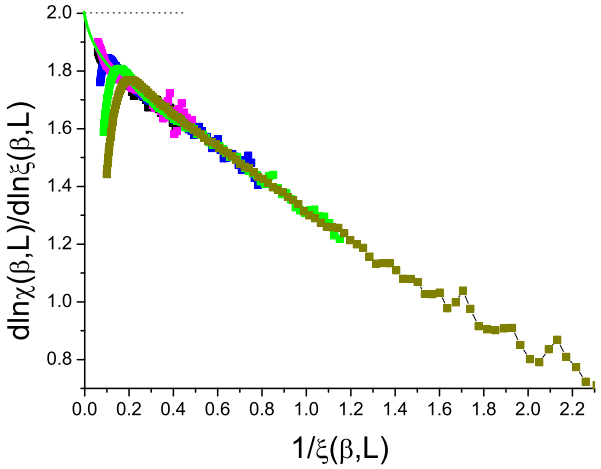

FIG. 1. (Color on line) The logarithmic derivative of the SG susceptibility by the second moment correlation length $\partial \ln \chi(\beta, L)/\partial \ln \xi(\beta, L)$ against the inverse correlation length $1/\xi(\beta, L)$ for the Laplacian model. $L = 128$, 96, 64, 48, 32 (left to right). Green continuous curve : extrapolation.

$\beta = (\langle J_{ij}^2 \rangle / T^2)^{1/2}$. The Ising spins are situated on simple $L \times L$ grids with periodic boundary conditions. The spin overlap parameter is defined as usual by

$$q = \frac{1}{L^d} \sum_i S_i^A S_i^B \tag{1}$$

where A and B indicate two copies of the same system and the sum is over all sites. The Laplacian interaction distribution is $P(J) = \sqrt{2} \exp(-\sqrt{2}|J|)$, and the uniform interaction distribution is $P(J) = 1/(2\sqrt{3})$ for $-\sqrt{3} < J < \sqrt{3}$. As in the Gaussian distribution, these distributions are continuous in the region around $J = 0$; each sample has a unique ground state and an anomalous dimension exponent $\eta \equiv 0$.

We first show in Fig. 1 and Fig. 2 $y(\beta, L) = \partial \ln \chi(\beta, L)/\partial \ln \xi(\beta, L)$ against $x(\beta, L) = 1/\xi(\beta, L)$ for these two models; the data can be compared with the data for the Gaussian model already shown in Ref. [1], Fig. 3. As must be the case for continuous distributions, the ThL envelope for the derivative in each of these models is consistent with an extrapolation to $y(\beta, L) = 2.0$ at zero temperature $x(\beta, L) = 0$, corresponding to the critical exponent $\eta = 0$ in each model.

In Fig. 3 we show the effective correlation length exponents $\nu_b(\beta, L) = \partial \ln[\xi(\beta, L)/\beta]/\partial \ln \tau(\beta)$ as functions of τ_b together for all sizes L and for all three continuous distribution models. In Fig. 4 we show the effective susceptibility exponents $\gamma_b(\beta, L) = \partial \ln \chi(\beta, L)/\partial \ln \tau(\beta)$ again for all L and for all three models. We have carried out extrapolations using just the same polynomial fit procedure as explained in detail in [1] and in the Appendix. The extrapolated zero temperature critical exponent estimates are $\nu_b = 1.27(2)$ and $\gamma_b = 3.52(5)$ for all three

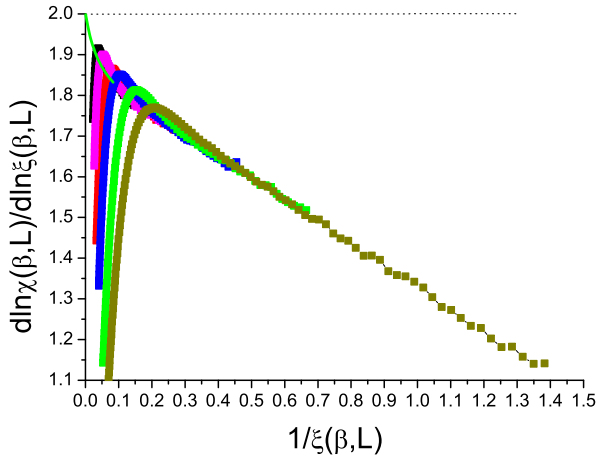

FIG. 2. (Color on line) The derivative of the SG susceptibility by the second moment correlation length $\partial \ln \chi(\beta, L)/\partial \ln \xi(\beta, L)$ against the inverse correlation length $1/\xi(\beta, L)$ for the uniform model. $L = 128$, 96, 64, 48, 32 (left to right). Green continuous curve : extrapolation.

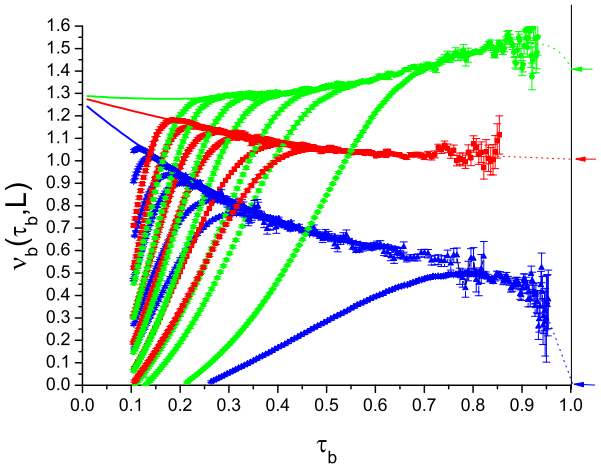

FIG. 3. (Color on line) The logarithmic derivative of the normalized second moment correlation length $\partial \ln[\xi(\tau_b)/\beta)]/\partial \ln \tau_b$ for the uniform (top sets, green circles), Gaussian (middle sets, red squares) and Laplacian (bottom sets, blue triangles), $L = 128$, 96, 64, 48, 32, 24, 8 (left to right in each case). Dashed curves : fits. Arrows : exact infinite temperature limits.

models. For all models (continuous and discrete interaction distributions) these critical exponents are related to the correlation length ν and anomalous dimension η critical exponents in the traditional T scaling convention by $\nu_b = (\nu - 1)/2$ and $\gamma_b = \nu(2 - \eta)/2$. The exact infinite temperature limits are $\nu_b = 2 - K/3$ where K is the kurtosis of the interaction distribution, and $\gamma_b = 4$ [1].

Thus all the critical exponent estimates for these three non-degenerate ground state models are compatible with $\eta = 0$ and $\nu = 3.52(2)$. We conclude that all two-dimensional non-degenerate ground-state ISG models lie in a single universality class; not only is $\eta = 0$ which must be true for this class of models, but also all critical ν values appear to be identical within the statistical and extrapolation errors. The strength and sign of the corrections to scaling are, however, quite different for the different models. Again, with the τ_b scaling convention, the correlation lengths with the leading Wegner scaling corrections assuming a leading correction exponent $\theta = 1$ are

$$\xi(\tau_b) = (0.69/\beta)\tau_b^{-1.28}[1 + 0.49\tau_b + \cdots] \qquad (2)$$

for the Gaussian model,

$$\xi(\tau_b) = (1.13/\beta)\tau_b^{-1.28}[1 - 0.04\tau_b + \cdots] \qquad (3)$$

for the uniform model, and

$$\xi(\tau_b) = (0.25/\beta)\tau_b^{-1.28}[1 + 2.5\tau_b + \cdots] \qquad (4)$$

for the Laplacian model.

It can be noted that these data provide a validation of the extrapolation procedure outlined in [1] and in the Appendix. Although the corrections are very different

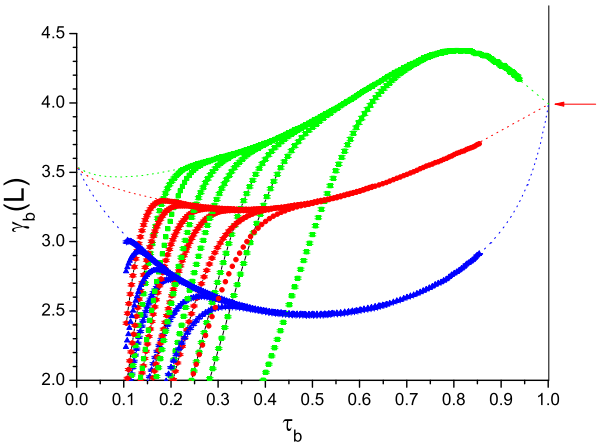

FIG. 4. (Color on line) The logarithmic derivative of the spin glass susceptibility $\partial \ln \chi(\tau_b)/\partial \ln \tau_b$ for the uniform (top sets, green circles), Gaussian (middle sets, red squares) and Laplacian (bottom sets, blue triangles), $L = 128, 96, 64, 48, 32, 24, 8$ (left to right in each case). Dashed curves : fits. Arrow : exact infinite temperature limit for all distributions.

in the three models, the extrapolations to criticality lead to consistent exponent values. *A priori* this implies that for other models where the same extrapolation procedure leads to other critical exponent estimates, these different values can be considered to be reliable.

IV. CORRELATION LENGTH RATIO AND BINDER CUMULANT SCALING

Universality in ISGs has been tested through comparing plots of the Binder parameter $g(\beta, L)$ against the second moment correlation length ratio $\xi(\beta, L)/L$ for different models, interpreted using finite size scaling arguments (see for instance Ref. [22]).

We will consider this type of scaling plot in the 2D context. In this section we will use $U_4(\beta, L) = 3 - 2g(\beta, L)$ rather than $g(\beta, L)$ to facilitate comparisons with Ref. [9].

Quite generally the 2D correlation function (either a spin-spin correlation function for ferromagnets or a spin glass correlation function for ISGs) at distance r takes the asymptotic form

$$G(\beta, r) \sim r^{-\eta} \exp[-r/\Xi(\beta)] \tag{5}$$

with possible small r finite size deviations, where $\Xi(\beta)$ is the exponential or "true" correlation length (not the second moment correlation length [26]). Dimensionless observables $Q(\beta, L)$ such as $U_4(\beta, L)$ or $\xi(\beta, L)/L$ will each be given by a general toroidal integral $Q(\beta, L) = \int^L F_Q(r) G(\beta, r) r^2 \mathrm{d}r$ where $F_Q(r)$ is the appropriate function for the variable, or a ratio of integrals.

For any model with $\eta = 0$ so $G(\beta, r) \sim \exp[-r/\Xi(\beta)]$, at given β and L the integrals are entirely determined by $\Xi(\beta)$ and L so whatever the temperature variations of $\Xi(\beta)$ for a particular model, plots of one dimensionless observable $Q_a(\beta, L)$ against another dimensionless observable $Q_b(\beta, L)$ will be universal, independent of the model and of L, in agreement with the general ISG scaling rule [22]. As the 2D models have $T_c = 0$ the universal curve for $\eta = 0$ models will extend up to the critical zero temperature limit $[U_4(0, L) = 1, \xi(0, L)/L = \infty]$ for all L.

The measurements on the $\eta = 0$ ISG models show that for small to moderate L and $\xi(\beta)/L < 0.3$, the $U_4(\beta, L)$ against $\xi(\beta, L)/L$ curves are not quite independent of L, Fig. 5. The small L deviations can be ascribed to the presence of pre-asymptotic corrections to $G(r)$. However, for $\xi(\beta)/L > 0.3$, the $U_4(\beta, L)$ against $\xi(\beta, L)/L$ scaling curves for the Gaussian, uniform and Laplacian $\eta = 0$ ISG models become identical and independent of L to within the statistics, Fig. 6. Only at very small sizes, $L \approx 4$, are there still weak finite size deviations, which were seen also in Ref. [9] for the Gaussian model. The present data show $L = 4$ deviations for the uniform model which are very similar in strength to the Gaussian deviations; the Laplacian model deviations are rather weaker.

In any model where η is not zero, at criticality $\Xi(\beta_c) = \infty$ and the critical observables will be given by integrals with the asymptotic correlation function $G(\beta_c, r) \sim r^{-\eta}$. (As this function diverges at $r = 0$, it must take up an appropriate functional form such as $G(\beta_c, r) = 1/(1 + r^\eta)$ for small r, leading to small L corrections). The explicit infinite size critical toroidal integrals for the 2D Ising ferromagnet with $\eta \equiv 1/4$ were calculated by Salas and Sokal [25], and gave $\xi(\beta_c, L)/L = 0.9050488292(4)$ and $U_4(\beta_c) = 1.16792\ldots$. For the 2D Fully Frustrated model with $\eta = 1/2$, from simulations there is a critical zero temperature end-point at $\xi(0, L)/L = 0.49(1)$, $U_4(0, L) = 1.615(5)$ ([27] and see Appendix I), with weak finite size effects. Numerical toroidal integrations for critical points could in principle be carried out for other η values. In 2D strip geometry at criticality $\xi(\beta_c, L)/L = 1/(\pi\eta)$ [28]. The Ising, FF and $\eta = 0$ values in square geometry correspond approximately to $\xi(\beta_c, L)/L = 1/(4.4\eta)$, and we can take this as a rough calibration for the estimation of the ISG η values from end-point $\xi(0, L)/L$ estimates.(Unfortunately all other partially frustrated $S = 1/2$ 2D Ising models have finite ordering temperatures and $\eta = 1/4$ like the Ising model [29] so can give no further critical point information).

For non-zero η ISG models with $T_c = 0$ one can expect $[U_4(0, L), \xi(0, L)/L]$ end-point limits for each L, with a critical zero temperature end-point limit for infinite L whose location will be determined uniquely by η.

In Fig. 6, $[U_4(0, L), \xi(0, L)/L]$ scaling plots are compared. In addition to a part of the $\eta = 0$ ISG universal scaling curve we show the 2D Ising ferromagnet T_c critical point, and scaling data for the 2D bimodal ISG. The Ising ferromagnet $\eta = 0.25$ critical point happens to lie rather close to the universal $\eta = 0$ curve. For the bimodal ISG model, data for each L can be seen to leave a common $\Xi(\beta)$ dominated regime curve (which is similar to but distinct from the $\eta = 0$ universal curve) before smoothly attaining a weakly L dependent end-point, corresponding to the $T < T^*(L)$ ground state regime. The observation that for each L this behavior is smooth and regular as the temperature tends to zero, with a final bunching up of data points when the ground state regime is reached, shows that the effective η in the $T > T^*(L)$ regime and in the (weakly L-dependent) $T < T^*(L)$ ground state regime are essentially the same. In other words the state degeneracy and hence η depends only mildly on temperature, right through the $T^*(L)$ crossover. The series of end-points for increasing L will terminate at an infinite L bimodal model end-point (see Ref. [17]) which is close to but beyond the ferromagnetic Ising critical point, so consistent with a bimodal ISG η which is lower than but close to $\eta = 0.25$. By inspection, the bimodal ISG data are totally incompatible with a critical exponent $\eta = 0$. The position of the infinite L bimodal ISG end-point will be estimated below together with the positions for three other discrete interaction distribution 2D ISG models, Fig. 16.

V. THE 2D BIMODAL ISG : THE QUOTIENT APPROACH

In Ref. [9] raw 2D Gaussian and bimodal ISG simulation data broadly equivalent to Ref. [1] were generated; these were analysed using a Quotient approach, with the normalized second moment correlation length

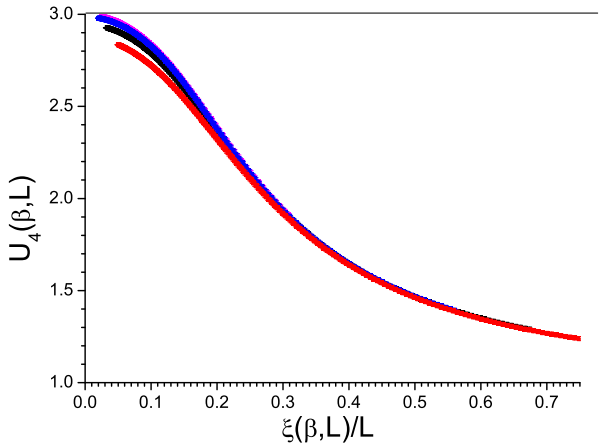

FIG. 5. (Color on line) Plot of the Binder cumulant $U_4(\beta, L)$ against $\xi(\beta, L)/L$ for the 2D Laplacian model from $\xi(\beta, L)/L = 0$ to $\xi(\beta, L)/L = 0.7$. $L = 48$, 12, 6, 4 (top to bottom). For all L the curves will extend to $U_4(\beta, L) = 1, \xi(\beta, L)/L = \infty$ at $T = 0$.

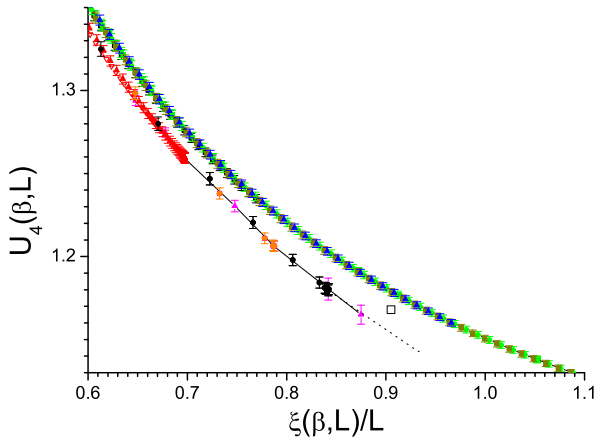

FIG. 6. (Color on line) Plot of the Binder cumulant $U_4(\beta, L)$ against $\xi(\beta, L)/L$ from $\xi(\beta, L)/L = 0.6$ to $\xi(\beta, L)/L = 1.1$. In the top curve, the 2D $L = 12$ Gaussian model (green circles), the 2D $L = 12$ uniform model (brown squares) and the 2D $L = 12$ Laplacian model (blue triangles), all overlapping. Lower set : the bimodal model, $L = 12$ red inverted triangles, $L = 16$ red triangles, $L = 32$ orange diamonds, $L = 48$ black circles, $L = 64$ pink triangles. Critical point 2D Ising ferromagnet : open square.

$x = \xi(T, L)/L$ as the scaling variable. It should be noted that the Quotients in Ref. [9] are at constant x not Quotients at constant T as in for instance Ref. [30]. Unfortunately no derivations are given in Ref. [9] for any of the important Quotient limit expressions which are cited. Here we provide simple derivations for the Quotient limits and we discuss plots made up of data formatted following the Quotient approach.

Assume the basic $T_c = 0$ scaling expressions $\xi(T) \sim T^{-\nu}$ and $\chi(T) \sim T^{-(2-\eta)\nu}$, valid near the large L, $T \to 0$ critical limit. At size L and temperature T, $x(T, L) = \xi(T, L)/L \sim T(x, L)^{-\nu}/L$.

Then for size $2L$ at the same x and at temperature $T''(x, 2L)$,

$$x(T'', 2L) = \frac{\xi(T'', 2L)}{2L} = \frac{T''(x, 2L)^{-\nu}}{2L} = \frac{T(x, L)^{-\nu}}{L} \tag{6}$$

with $x(T, L) = x(T'', 2L)$; so $T(x, L)^{-\nu}/T''(x, 2L)^{-\nu} = 2$ i.e. the Quotient Q_T as defined in Ref. [9] tends to

$$Q_T = \frac{T''(x, 2L)}{T(x, L)} = 2^{-1/\nu} \tag{7}$$

in the large L limit. This expression is identical to the limit relation cited in Ref. [9] Eqn. (7), implying that the limit derivation procedure followed was the same as the present one. Using this expression, the Gaussian $Q_T(0) = 0.82$ large L intercept reported in Ref. [9] is consistent with the accepted literature value $\nu = 3.55(2)$ [4–8] for the Gaussian ISG critical exponent.

Then

$$\langle q^2 \rangle(T, L) = \frac{\chi(T, L)}{L^2} = \frac{T^{-(2-\eta)\nu}}{L^2} \tag{8}$$

With $x = \xi(L, T)/L$, from above $T(x, L)^{-\nu} = \xi(T, L) = Lx(T, L)$, so

$$\langle q^2 \rangle(x, L) = \frac{T(x, L)^{-\nu(2-\eta)}}{L^2} = \frac{(xL)^{(2-\eta)}}{L^2} = L(x, T)^{-\eta} x^{2-\eta} \tag{9}$$

i.e. the Quotient $Q_{q^2} = \langle q^2 \rangle(x, 2L)/\langle q^2 \rangle(x, L) = 2^{-\eta}$ in the large L limit. This is identical to the expression cited in Ref. [9], Eqn. (D3).

We can inspect Figs. 7 and 8 for the bimodal ISG Quotients with points compiled from the present numerical data; the figures are presented in just the same form as Ref. [9] Fig. 7 upper and middle. As far as can be judged by reading off the plots in Ref. [9], point by point agreement between the present Quotients and those of Ref. [9] is excellent (as could be expected as the raw data should be essentially the same). The natural extrapolations indicated in the present figures lead to bimodal ISG critical infinite-L Quotient intercept estimates $Q_T(0) = 0.865(10)$ and $Q_{q^2}(0) = 0.87(1)$. (No equivalent extrapolations of the bimodal Quotient data were made in Ref. [9], but if these had been made the intercept estimates would have been very similar to the present values). From the limit expressions above, these intercepts correspond to bimodal critical exponent estimates $\nu = 4.8(3)$ and $\eta = 0.20(2)$, estimates which are fully consistent with the bimodal exponents estimated through a completely independent analysis procedure in

Ref. [1]. In particular the value obtained for η is clearly non-zero.

Finally, in Ref. [9] section VI and Appendix C an observable $g(x,T)$ is defined by $g(x,T) = \langle q^2\rangle(x = 0.4,T)/\langle q^2\rangle(x,T)$ averaged over T. (The factor $[\hat{u}_h(T)]^2$ depends only on T and so cancels out in the ratio in Ref. [9] Fig. 3). Note that the $\langle q^2\rangle(x = 0.4,T)$ and $\langle q^2\rangle(x,T)$ in the definition of $g(x,T)$ correspond to the same T but at quite different L, say $L(x,T)$ and $L''(0.4,T)$.

From the Quotient discussion for Q_{q^2} above and assuming some fixed T: $\langle q^2\rangle(x,T) = L(x,T)^{-\eta}x^{2-\eta}$ and from the Q_T discussion $L(x,T) = T(x,L)^{-\nu}/x(T,L)$.

So :

$$\begin{aligned}\langle q^2\rangle(x=0.4,T) &= \overbrace{[T(0.4,L'')^{-\nu}/0.4]}^{T(x,L'')^{-\nu}/x(T,L'')}{}^{-\eta}0.4^{2-\eta}\\ &= [T(0.4,L'')^{-\nu}]^{-\eta}0.4^{\eta}0.4^{2-\eta}\\ &= [T(0.4,L'')^{-\nu}]^{-\eta}0.4^{2} \qquad (10)\end{aligned}$$

and

$$\begin{aligned}\langle q^2\rangle(x,T) &= [T(x,L)^{-\nu}/x(T,L)]^{-\eta}x^{2-\eta}\\ &= [T(x,L)^{-\nu}]^{-\eta}x^{\eta}x^{2-\eta}\\ &= [T(x,L)^{-\nu}]^{-\eta}x^{2} \qquad (11)\end{aligned}$$

As $T(0.4,L'') = T(x,L)$,

$$g(x,T) = \frac{\langle q^2\rangle(0.4,T)}{\langle q^2\rangle(x,T)} = 0.4^2x^{-2} = \frac{0.16}{x^2} \qquad (12)$$

at small x whatever η. The log-log $g(x,T)$ against x data plot shown in Ref. [9] Fig. 3 is entirely consistent with this simple rule (including the pre-factor 0.16) from $x = 0.1$ to about $x = 0.5$ for both the Gaussian and the bimodal models.

The relation $g(x) \sim 1/x^{2-\eta}$ cited (with no derivation) in Ref. [9] is in disagreement with the present derivation, and with the observed data shown in Ref. [9]. The conclusion in Ref. [9] that $|\eta| < 0.02$ for the 2D bimodal ISG model, drawn principally from $g(x,T)$ analyses, seems to have been based on an incorrect expression and so is invalid.

To summarize, when the Quotient analyses presented in Ref. [9] with the limit derivations given above are applied to the bimodal simulation data, estimates for the critical exponents in the bimodal ISG model obtained by extrapolations of $Q(T)$ and $Q(q^2)$ to large L are consistent with those obtained following the analysis procedure used in Ref. [1]. Both bimodal exponents are quite different from the values for the continuous distribution models. The $g(x,T)$ data analysis provides no information on the critical exponents.

VI. DISCRETE INTERACTION DISTRIBUTION ISGS

Having studied the standard 2D bimodal model in [1], we have now made equivalent measurements on three different degenerate ground state models : a diluted bimodal model with a fraction $p = 0.125$ of the interactions set randomly to zero (a diluted bimodal model was already studied in Refs. [19, 31]), an "anti-diluted" bimodal model where a fraction $p = 0.2$ of the interactions are set randomly to strength $\pm 2J$ and the remaining fraction to $\pm J$. Also we test a more complex symmetric Poisson model with an interaction distribution shown in Fig. 9; this model has probability $\lambda^{|k|}\exp(-\lambda)/2$ for strength $(k/4)J$, when $k \neq 0$, and probability $\exp(-\lambda)$

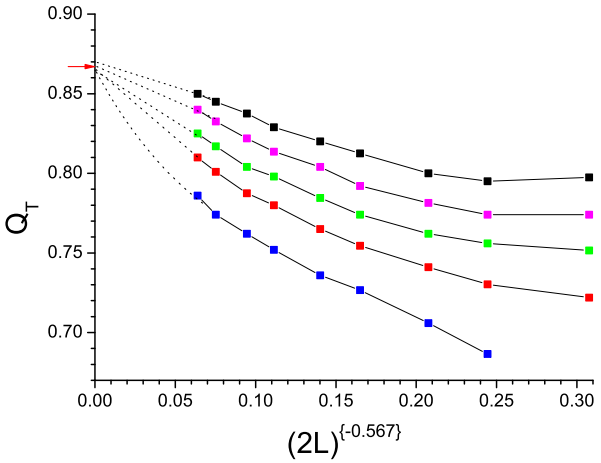

FIG. 7. (Color on line) The 2D bimodal Quotient $Q_T(x,L)$ for $x = \xi(L)/L$ values $x = 0.1$, 0.2, 0.3, 0.4, 0.5 (bottom to top). The horizontal axis is $(2L)^{-0.567}$ as in Ref. [9] (In this reference the axis is stated to be $(L)^{-0.567}$ which is incorrect).

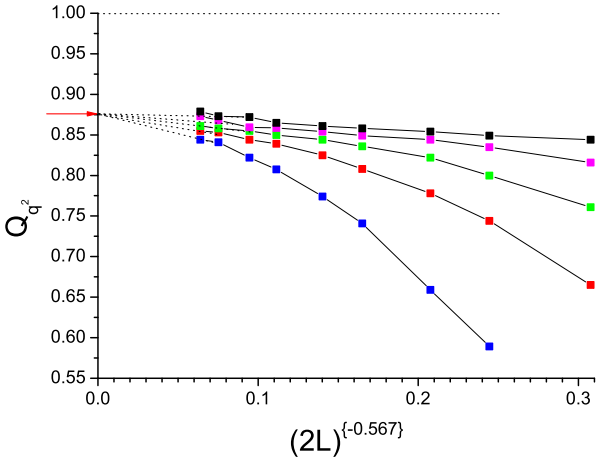

FIG. 8. (Color on line) The 2D bimodal Quotient $Q_{q^2}(x,L)$ for $x = \xi(L)/L$ values $x = 0.1$, 0.2, 0.3, 0.4, 0.5 (bottom to top). The horizontal axis is $(2L)^{-0.567}$ as in Ref. [9] (In this reference the axis is stated to be $(L)^{-0.567}$ which is incorrect).

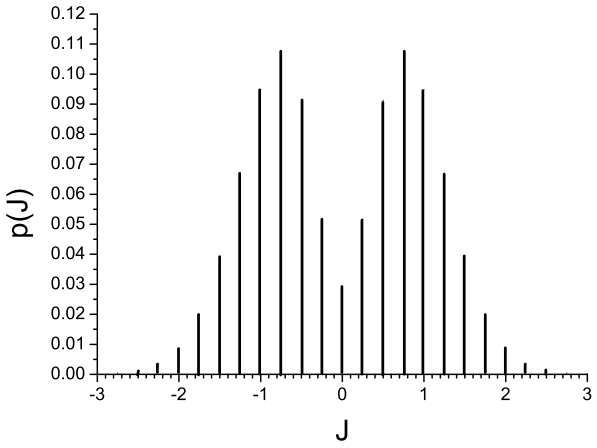

FIG. 9. (Color on line) The interaction distribution for the symmetric Poisson ISG model.

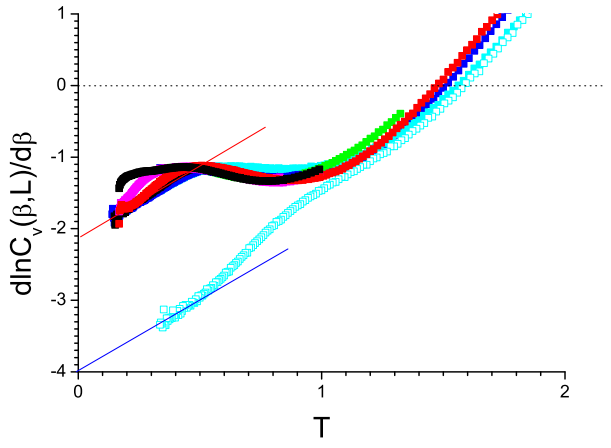

FIG. 10. (Color on line) Diluted bimodal 2D ISG. Logarithmic derivative of the specific heat $\partial \ln C_v(\beta, L)/\partial\beta$ against T. Full points : $L = 32, 24, 16, 12, 6, 4$ (green, black, pink, red, blue, cyan; top to bottom on the right). Open points : bimodal 2D ISG $L = 4$ for comparison. Red line : $y(x) = -2.1 + 2x$, blue (lower) line $y(x) = -4 + 2x$.

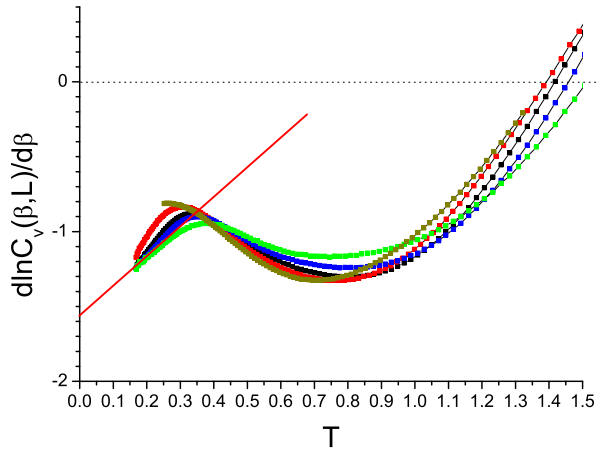

FIG. 11. (Color on line) "Anti-diluted" bimodal 2D ISG. Logarithmic derivative of the specific heat $\partial \ln C_v(\beta, L)/\partial\beta$ against T. Full points : $L = 24, 12, 8, 6, 4$ (brown, red, black, blue, green; top to bottom on the right). Red line : $y(x) = -1.55 + 2x$.

when $k = 0$, with $\lambda = (\sqrt{65} - 1)/2$.

These models have discrete interaction distributions and so can be expected to have degenerate ground states; we do not, however, know the values of the ground state degeneracy. Logarithmic derivatives of the specific heat data are shown in Figs. 10, 11 and 12 in the same format, $\partial \ln C_v/\partial\beta$ against T, as that of the bimodal ISG model in [1] Fig. 4 and of the FF model, Fig. 26 below. Again the discrete distribution data indicate crossovers for all models, with a $T < T^*(L)$ ground state plus gap regime specific heat of the form $C_v \sim \beta^B \exp(-A\beta)$ having $B \approx 2$. The effective gap parameter $A \approx 2.1$ for the diluted bimodal model, $A \approx 1.5$ for the anti-diluted bimodal model, and $A \approx 0.5$ for the symmetric Poisson model, so significantly smaller than the gap $A = 4$ of both the FF and pure bimodal models. Ref. [31] showed data on a perturbed FF model which were also interpreted as having a gap A weaker than 4. We do not dispose of large L data to low enough T to be able to establish the limiting infinite size $T > T^*(L)$ ThL form of $C_v(T)$ for these models.

In each of the discrete interaction models, the normalized correlation length saturates at an end-point value at low temperature for all L. As an example the data for the symmetric Poisson model are shown in Fig. 13. Binder cumulant $U_4(\beta, L)$ against normalized correlation length $\xi(\beta, L)/L$ plots are shown in Figs. 14 and 15 for the diluted bimodal and anti-diluted bimodal models. As for the bimodal model the data points lie on a curve distinct from the continuous distribution universal curve and tend to end-points for each L at zero temperature, behavior characteristic of a non-zero exponent η. The end-point values of $\xi(0, L)/L$ for all four discrete interaction models are shown plotted against $1/L$ in Fig. 16. The infinite L end-point values estimated by extrapolation are distinct, indicating that the η values are distinct so the discrete interaction models are all in different universality classes.

From the approximate calibration of the $[\xi(L)/L]_{T=0}$ infinite L end-point values in terms of η above, we can give estimates $\eta \approx 0.24, 0.21, 0.18, 0.14$ respectively for the bimodal, diluted, anti-diluted and symmetric Poisson models. We can remark that the end point values lie close to but beyond the 2D Ising ferromagnet critical value, implying the ISG η values are all near to but somewhat below 0.25. The η values are roughly consistent with the

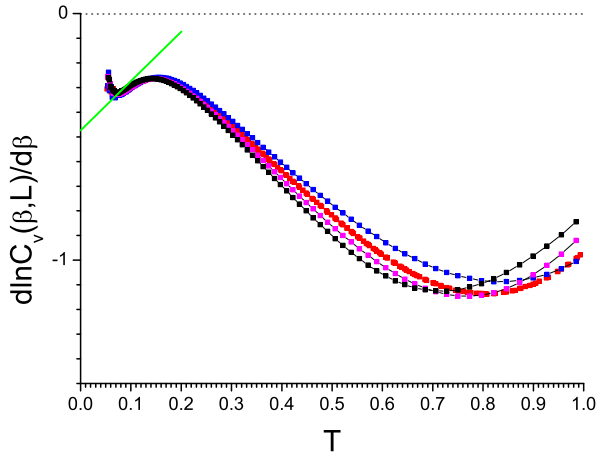

FIG. 12. (Color on line) Symmetric Poisson 2D ISG. Logarithmic derivative of the specific heat $\partial \ln C_v(\beta, L)/\partial\beta$ against T. Full points : $L = 24$, 12, 8, 6 (black, pink, red, blue; top to bottom on the right). Green line : $y(x) = -0.45 + 2x$.

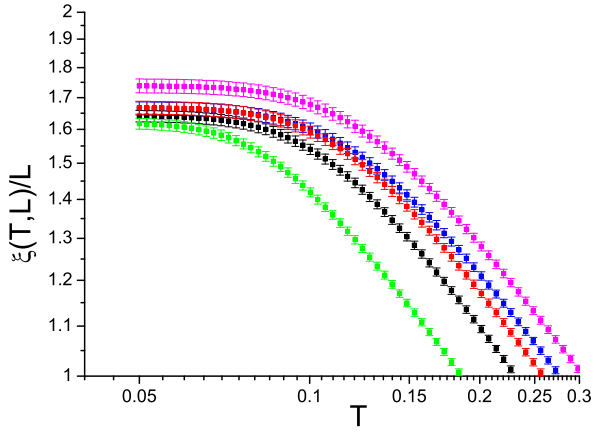

FIG. 13. (Color on line) Symmetric Poisson 2D ISG. The normalized correlation length $\xi(T, L)/L$ against T at low temperatures. $L = 4$, 6, 8, 12, 24 (top to bottom).

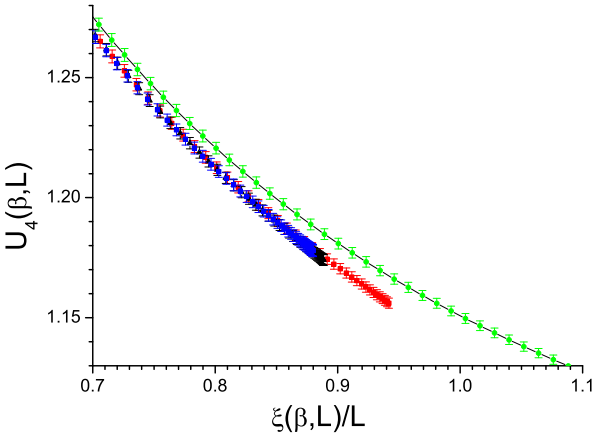

FIG. 14. (Color on line) Diluted bimodal 2D ISG. The low temperature Binder cumulant $U_4(\beta, L)$ against the normalized correlation length $\xi(\beta, L)/L$. ($L = 24$ red squares, $L = 12$ black triangles, $L = 8$ blue diamonds). For each L the data points terminate at a zero temperature end-point. For comparison, the universal continuous distribution curve is represented by $L = 12$ Gaussian ISG data (upper set, green circles) which extend to infinity.

η estimates from a diferent approach given below.

In Figs. 17, 18 and 19 we show the $y(\beta, L) = \partial \ln \chi(\beta, L)/\partial \ln \xi(\beta, L)$ against $x(\beta, L) = 1/\xi(\beta, L)$ plots for the diluted bimodal, the "anti-diluted" bimodal and the symmetric Poisson model. By mild extrapolation the intercepts can be estimated to be $y(x = 0) \approx 1.845$, 1.87 and 1.90 , i.e. $\eta = 2 - y(x = 0) \approx 0.155(10)$, 0.13(1) and 0.10(1) for these models, weaker than the estimate $\eta = 0.20(2)$ for the bimodal model [1], but still far from zero. As in the bimodal ISG, there are overshoots as functions of temperature for individual L curves. (In Ref. [19], for a diluted bimodal model at zero temperature the estimate obtained was $\eta \approx 0.20$).

In Figs. 20, 21, and 22 we show the effective exponent $\nu_b(\beta, L) = \partial \ln[\xi(\beta, L)/\beta]/\partial \ln \tau_b$ for all sizes L for these models, and in Figs. 23, 24 and 25 we show the effective exponents $\gamma_b(\beta, L) = \partial \ln \chi(\beta, L)/\partial \ln \tau_b$. We have carried out extrapolations using just the same polynomial fit procedure as explained in [1] and in the Appendix in order to estimate the zero temperature critical intercepts.

The extrapolated critical exponent estimates for the diluted bimodal model, the anti-diluted bimodal model, and the symmetric Poisson model are $\nu_b = 1.40(2)$, 1.39(2), 1.30(2) and $\gamma_b = 3.65(5)$, 3.60(5), 3.46(2) respectively, as compared with $\nu_b = 1.9(1)$, $\gamma_b = 4.3(1)$ for the bimodal model [1]. These exponents are related to the correlation length critical exponent ν in the traditional T scaling convention by $\nu_b = (\nu - 1)/2$ and $\gamma_b = \nu(2 - \eta)/2$ [1]. Thus the critical exponent estimates for the degenerate ground state models are consistent with $\eta = 0.155(5)$, $\nu = 3.8(1)$, $\eta = 0.13(1)$, $\nu = 3.7(2)$, and $\eta = 0.10(2)$, $\nu = 3.6(1)$ respectively, as compared with $\eta = 0.20(2)$, $\nu = 4.8(1)$ for the bimodal model (and $\eta = 0$, $\nu = 3.55(2)$ for the continuous distribution models). The data for the bimodal model true correlation length at low temperatures obtained by Merz and Chalker with a remarkable network mapping technique, Ref. [37] Fig. 24, can be extrapolated to a critical exponent value $\nu \approx 4.6$ which is consistent with the simulation estimate for the bimodal value ν in Ref. [1].

Although these values are similar to each other they are all different and all are quite distinct from the bimodal model estimates $\eta = 0.20(2), \nu = 4.8(3)$, [1].

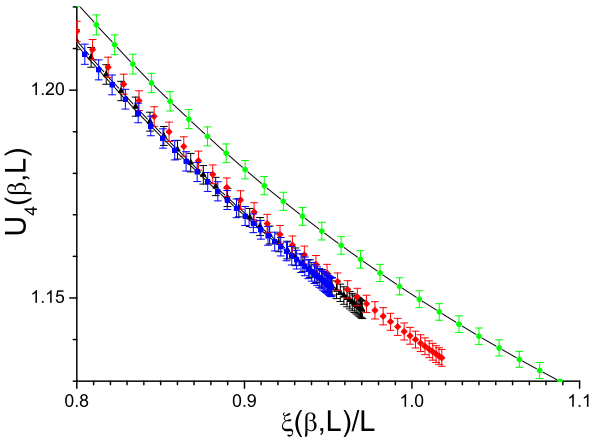

FIG. 15. (Color on line) Anti-diluted bimodal 2D ISG. The low temperature Binder cumulant $U_4(\beta, L)$ against the normalized correlation length $\xi(\beta, L)/L$. ($L = 12$ red diamonds, $L = 8$ black triangles, $L = 6$ blue squares). For each L the data points terminate at a zero temperature end-point. For comparison, the universal continuous distribution curve is represented by $L = 12$ Gaussian ISG data (upper set, green circles) which extend to infinity.

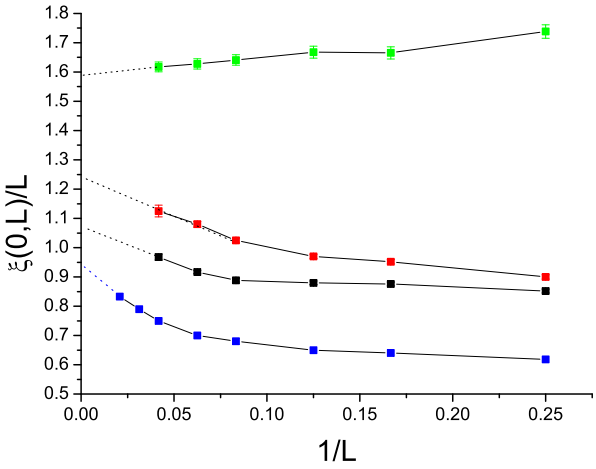

FIG. 16. (Color on line) The size dependent zero temperature end-point values of $\xi(\beta, L)/L$ for the four discrete interaction models : the symmetric Poisson model, the anti-diluted bimodal model, the diluted bimodal model, and the bimodal model, from top to bottom.

VII. CONCLUSIONS

We show simulation data for three continuous and four discrete interaction distribution 2D ISG models and for the 2D fully frustrated Villain model (Appendix I). All these models order only at zero temperature. The simulation techniques and the analysis follow strictly those of Ref. [1] where results for the canonical 2D ISG bimodal (discrete) and Gaussian (continuous) interaction distribution models were reported. We have made extensive simulation measurements up to size $L = 128$ on each model, which have been analysed using the 2D scaling parameter $\tau_b = 1/(1 + \beta^2)$ as in [1] as well as the traditional scaling parameter T.

In the class of ISG models with continuous interaction distributions, in addition to the Gaussian distribution we have studied the uniform interaction distribution and the

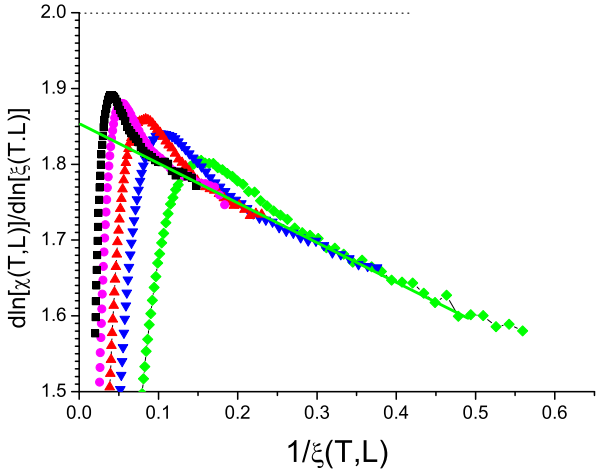

FIG. 17. (Color on line) Diluted bimodal 2D ISG. Logarithmic derivative $\partial \ln \chi(\beta, L)/\partial \ln \xi(\beta, L)$ against $1/\xi(\beta, L)$ for $L = 128$, 96, 64, 48, 32 (black, pink, red, blue, green) left to right. The continuous (green) curve is an extrapolated fit.

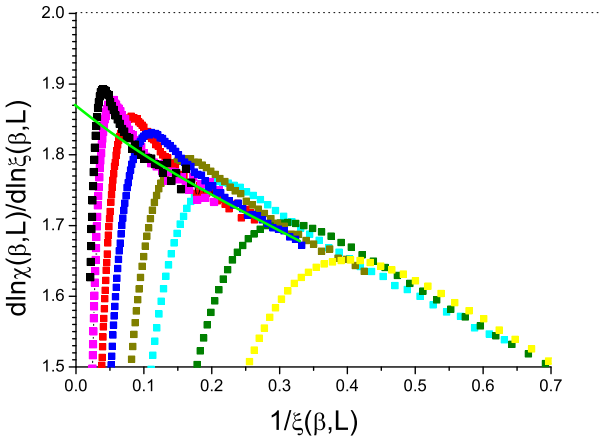

FIG. 18. (Color on line) Anti-diluted bimodal 2D ISG. Logarithmic derivative $\partial \ln \chi(\beta, L)/\partial \ln \xi(\beta, L)$ against $1/\xi(\beta, L)$ for $L = 128$, 96, 48, 32, 24, 16, 12 (left to right). The continuous (green) curve is an extrapolated fit.

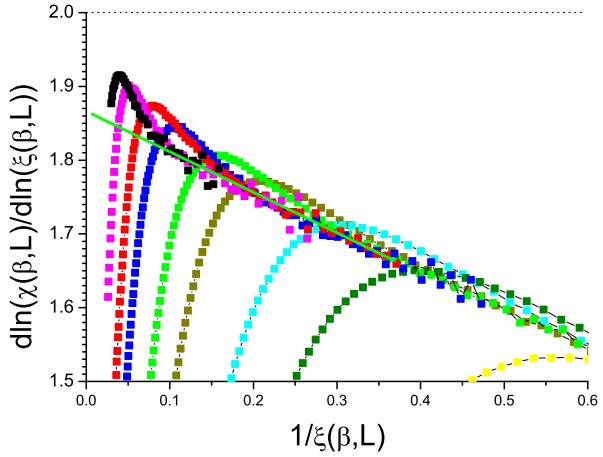

FIG. 19. (Color on line) Symmetric Poisson 2D ISG. Logarithmic derivative $\partial \ln \chi(\beta, L)/\partial \ln \xi(\beta, L)$ against $1/\xi(\beta, L)$ for $L = 128$, 96, 48, 32, 24, 16, 12, 8 (left to right).

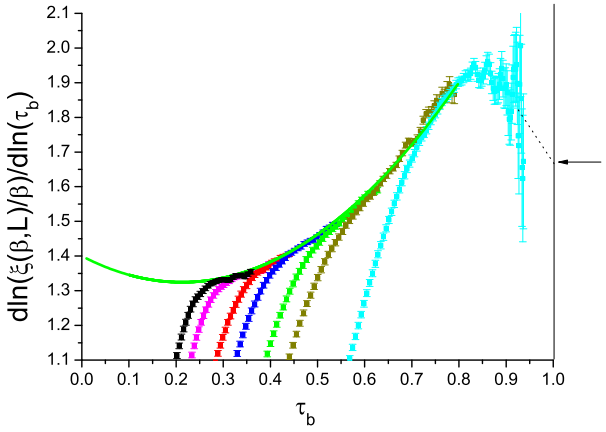

FIG. 20. (Color on line) Diluted bimodal 2D ISG. Logarithmic derivative $\partial \ln[\xi(\beta, L)/\beta]/\partial \ln \tau_b$ against τ_b for $L = 128$, 96, 64, 48, 32, 24, 12 (left to right). The continuous (green) curve is an extrapolated fit. The right hand side arrow indicates the exact infinite temperature limit.

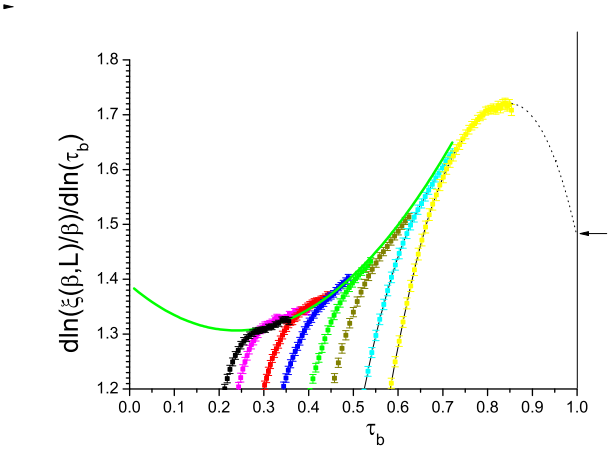

FIG. 21. (Color on line) Anti-diluted bimodal 2D ISG. Logarithmic derivative $\partial \ln[\xi(\beta, L)/\beta]/\partial \ln \tau_b$ against τ_b for $L = 128$, 96, 48, 32, 24, 16, 12 (left to right). The continuous (green) curve is an extrapolated fit. The right hand side arrow indicates the exact infinite temperature limit.

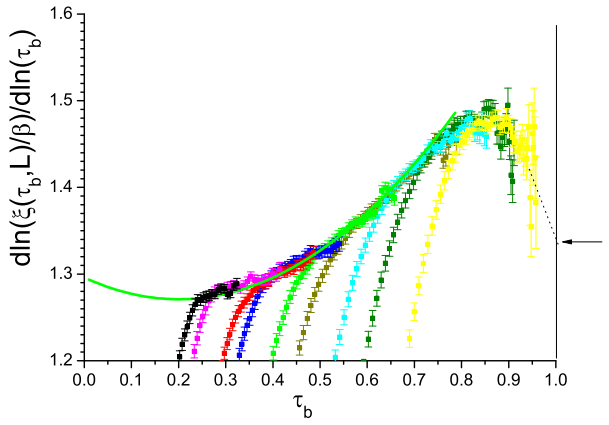

FIG. 22. (Color on line) Symmetric Poisson 2D ISG. Logarithmic derivative $\partial \ln[\xi(\beta, L)/\beta]/\partial \ln \tau_b$ against τ_b for $L = 128$, 96, 48, 32, 24, 16, 12, 8 (left to right). The continuous (green) curve is an extrapolated fit. The right hand side arrow indicates the exact infinite temperature limit.

Laplacian interaction distribution. These models have non-degenerate ground states and as a consequence an anomalous dimension exponent $\eta \equiv 0$. Except for very small sizes and high temperatures, for all $\eta = 0$ models and for all L, Binder parameter $U_4(\beta, L)$ against normalized second moment correlation length $\xi(\beta, L)/L$ data lie on a single universal curve extending to the zero temperature limit $[U_4(L) = 1, \xi(L)/L \equiv \infty]$.

The present numerical data show that estimates for the critical second moment correlation length exponent for the continuous interaction distributions are all compatible with $\nu = 3.55(2)$ (expressed in terms of the T temperature scaling convention), which is the accepted value for the Gaussian distribution 2D ISG [4–8]. This result is consistent with all continuous interaction distribution 2D ISGs forming a single universality class.

The bimodal interaction 2D ISG, a diluted bimodal interaction 2D ISG, an "anti-diluted" 2D ISG, a multi-peak 2D ISG, and the 2D FF model, all order only at zero temperature, have discrete interaction distributions, and have highly degenerate ground states. For each model the specific heat data show crossovers at size dependent temperatures $T^*(L)$ between an effectively continu-

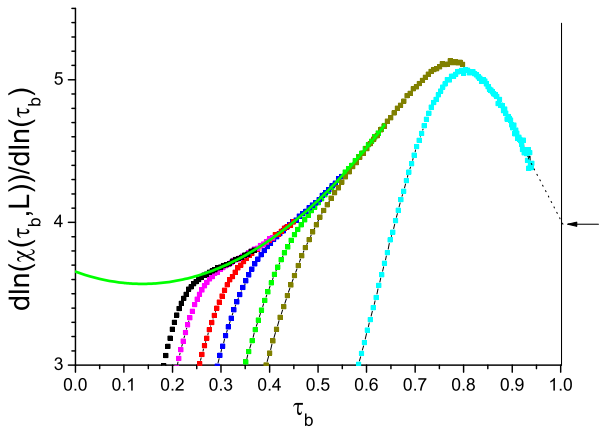

FIG. 23. (Color on line) Diluted bimodal 2D ISG. Logarithmic derivative $\partial \ln \chi(\beta, L)/\partial \ln \tau_b$ against τ_b for $L = 128$, 96, 48, 32, 24 (left to right). The continuous (green) curve is an extrapolated fit. The right hand side arrow indicates the exact infinite temperature limit.

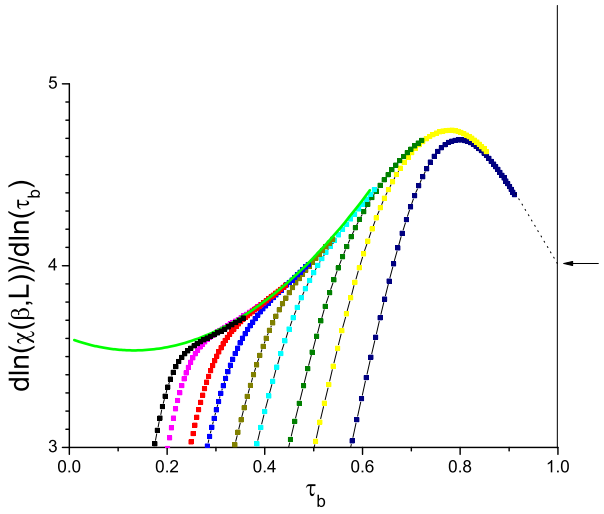

FIG. 24. (Color on line) Anti-diluted bimodal 2d ISG. Logarithmic derivative $\partial \ln \chi(\beta, L)/\partial \ln \tau_b$ against τ_b for $L = 128$, 96, 48, 32, 24, 16, 12 (left to right). The continuous (green) curve is an extrapolated fit. The right hand side arrow indicates the exact infinite temperature limit.

ous energy state distribution regime for $T > T^*(L)$ and a ground state plus excited state dominated regime for $T < T^*(L)$. For each of these models, Binder parameter $U_4(\beta, L)$ against normalized second moment correlation length $\xi(\beta, L)/L$ data do not lie on the $\eta = 0$ universal curve, and for every L the data tend to zero temperature end-points which are far from $U_4(L) = 1$, $\xi(L)/L \equiv \infty$. As the temperature is lowered the data evolve continuously and smoothly through T^* indicating that the effective η values in the $T > T^*(L)$ and $T < T^*(L)$ regimes are the same. The end point values of $\xi(L)/L$ extrapolated to infinite L are different for each model, implying that the models all lie in different universality classes with different non-zero η values.

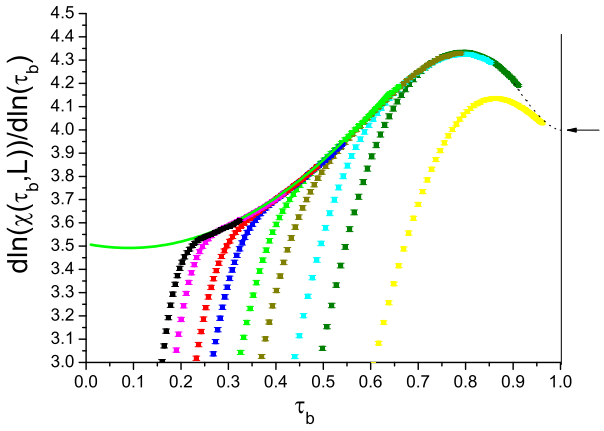

FIG. 25. (Color on line) Symmetric Poisson 2d ISG. Logarithmic derivative $\partial \ln \chi(\beta, L)/\partial \ln \tau_b$ against τ_b for $L = 128$, 96, 48, 32, 24, 16, 12, 8 (left to right). The continuous (green) curve is an extrapolated fit. The right hand side arrow indicates the exact infinite temperature limit.

From scaling analyses, the critical exponents of the discrete distribution ISGs are estimated to be $\eta = 0.20(2)$, $\nu = 4.8(1)$ for the bimodal model, $\eta = 0.155(5)$, $\nu = 3.8(1)$ for the $p = 0.125$ diluted bimodal model, $\eta = 0.13(1)$, $\nu = 3.8(1)$ for the $p = 0.20$ anti-diluted bimodal model, and $\eta = 0.10(1)$, $\nu = 3.6(1)$ for the symmetric Poisson model defined above.

Each of the present discrete distribution models represents an infinite family of possible models. If a parameter defining a particular model was modified (for instance by choosing other values of p for the diluted or anti-diluted models) we would expect the critical exponents to change continuously as functions of p, starting of course from the bimodal values for $p = 0$.

To summarize, the 2D ISG models with continuous interaction distributions lie in a single universality class, but the 2D ISG models with discrete distributions do not share this universality class. On the contrary each discrete distribution model has its individual critical exponents.

When it was reported in 1980 by Morgenstern and Binder [11] that the 2D bimodal ISG had a value $\eta = 0.4(1)$ which is non-zero so different from the $\eta \equiv 0$ of the Gaussian model, it was suggested that this universality breakdown behavior could arise from higher order terms in the ϵ-expansion for the critical exponents in dimensions below upper critical dimension $d = 6$ [32], see also [33]. Indeed there is now numerical evidence for non-universality in dimensions $d = 4$ [34, 35] and $d = 5$ [36]

as well as in dimension $d = 2$.

ACKNOWLEDGMENTS

We thank Helmut Katzgraber for generously giving us access to all the raw Fully Frustrated data originally generated for Ref. [27], and to the raw low temperature bimodal ISG data originally generated for Ref. [17]. We would like to thank Mike Moore for pointing out references [32], [33] and [37], and John Chalker for helpful comments. The computations were performed on resources provided by the Swedish National Infrastructure for Computing (SNIC) at the Chalmers Centre for Computational Science and Engineering (C3SE).

[1] P. H. Lundow and I. A. Campbell, Phys. Rev. E **93**, 022119 (2016).
[2] A. K. Hartmann and A. P. Young, Phys. Rev. B 64, 180404(R) (2001).
[3] M. Ohzeki and H. Nishimori, J. Phys. A: Math. Theor. 42, 332001 (2009).
[4] H. Rieger, L. Santen, U. Blasum, M. Diehl, M. Jünger, and G. Rinaldi, J. Phys. A **29**, 3939 (1996); 30, 8795(E) (1997).
[5] A. K. Hartmann and A. P. Young, Phys. Rev. B **66**, 094419 (2002).
[6] A. C. Carter, A. J. Bray, and M. A. Moore, Phys. Rev. Lett. **88**, 077201 (2002).
[7] A. K. Hartmann, A. J. Bray, A. C. Carter, M. A. Moore, and A. P. Young, Phys. Rev. B **66**, 224401 (2002).
[8] J. Houdayer and A. K. Hartmann, Phys. Rev. B **70**, 014418 (2004).
[9] L. A. Fernandez, E. Marinari, V. Martin-Mayor, G. Parisi, and J. J. Ruiz-Lorenzo, Phys. Rev. B **94**, 024402 (2016).
[10] T. Jörg, J. Lukic, E. Marinari, and O. C. Martin, Phys. Rev. Lett. **96**, 237205 (2006).
[11] I. Morgenstern and K. Binder, Phys. Rev. B **22**, 288 (1980).
[12] W. L. McMillan, Phys. Rev. B **28**, 5216 (1983).
[13] J.-S. Wang and R. H. Swendsen, Phys. Rev. B **37**, 7745 (1988).
[14] Y. Ozeki, J. Phys. Soc. Jpn. 59, 3531 (1990).
[15] J. Houdayer, Eur. Phys. J. B **22**, 479 (2001).
[16] H. G. Katzgraber and Lik Wee Lee, Phys. Rev. B **71**, 134404 (2005).
[17] H. G. Katzgraber, Lik Wee Lee, and I. A. Campbell, Phys. Rev. B **75**, 014412 (2007).
[18] J. Poulter and J. A. Blackman, Phys. Rev. B **72**, 104422 (2005).
[19] A. K. Hartmann, Phys. Rev. B **77**, 144418 (2008).
[20] F. Parisen Toldin, A. Pelissetto, and E. Vicari, Phys. Rev. E **82**, 021106 (2010).
[21] F. Parisen Toldin, A. Pelissetto, and E. Vicari, Phys. Rev. E **84**, 051116 (2011).
[22] T. Jörg, Phys. Rev. B **73**, 224431 (2006).
[23] F. J. Wegner, Phys. Rev. B **5**, 4529 (1972).
[24] I. A. Campbell, K. Hukushima, and H. Takayama, Phys. Rev. Lett. **97**, 117202 (2006), Phys. Rev. B **76**, 134421 (2007).
[25] J. Salas and A. D. Sokal, J.Stat.Phys. **98**, 551 (2000).
[26] P. Butera and M. Comi, Phys. Rev. B **69**, 174416 (2004).
[27] H. G. Katzgraber, I. A. Campbell, and A. K. Hartmann, Phys. Rev. B **78**, 184409 (2008).
[28] J. L. Cardy, J. Phys. A **17**, L961 (1984).
[29] J. Wu and D. Mattis, Phys. Rev. B **67**, 224414 (2003).
[30] H. G. Ballesteros, A. Cruz, L. A. Fernandez, V. Martin-Mayor, J. Pech, J. J. Ruiz-Lorenzo, A. Tarancon, P. Tellez, C. L. Ullod, and C. Ungil, Phys. Rev. B **62**, 14237 (2000).
[31] J. Lukic, E. Marinari, and O. C. Martin, Europhys. Lett. **73**, 779 (2006).
[32] A. J. Bray and M. A. Moore J. Phys. C: Solid State Phys., **14**, 1313 (1981).
[33] D. J. Elderfield and A. J. McKane, Phys. Rev. B **18**, 3730 (1978).
[34] P. H. Lundow and I. A. Campbell, Phys. Rev. E **91**, 042121 (2015).
[35] P. H. Lundow and I. A. Campbell, Physica A **434**, 181 (2015).
[36] P. H. Lundow and I. A. Campbell, arXiv:1606.03108 (Accepted for publication in Phys. Rev. E).
[37] F. Merz and J. T. Chalker, Phys. Rev. B **65**, 054425 (2002).
[38] J. Villain, J. Phys. C **10**, 1717 (1977).
[39] G. Forgacs, Phys. Rev. B **22**, 4473 (1980).
[40] C. K. Thomas and A. A. Middleton, Phys. Rev. B 76, 220406(R) (2007).
[41] C. K. Thomas, D. A. Huse, and A. A. Middleton, Phys. Rev. Lett. **107**, 047203 (2011).

Appendix A: The fully frustrated Villain model

In the square lattice fully frustrated (FF) Villain model [38] all near neighbor interactions have strength $|J|$; in the x direction all bonds are ferromagnetic, while in the y direction columns of bonds are alternately ferromagnetic and antiferromagnetic, so every plaquette is frustrated. This is a well understood 2D model with a zero temperature ferromagnetic transition and a strong ground state degeneracy, which can provide a basis of comparison for other models with ground state degeneracies such as discrete interaction distribution ISG models.

For the FF model a number of properties have been established analytically [39], by precise energy measurements [31], and by simulations [27]. The FF ground state degeneracy corresponds to a zero temperature entropy per site of 0.2916 [39]. (For comparison in the 2D bimodal ISG the zero temperature entropy per site is 0.078(5) [5, 18, 40]). The first FF excited states are at $4J$. The zero temperature FF ordering is ferromagnetic, with a thermodynamic limit ($L = \infty$, $T = 0$) anomalous dimension exponent $\eta \equiv 1/2$ [39] and a low

temperature thermodynamic limit second moment correlation length $\xi(\beta) \sim \exp(2\beta)/2$ [27, 31, 39]. The FF specific heats in the infinite L and finite L limits were estimated in Ref. [31] by sophisticated Pfaffian algebra to be of the form $C_v \sim \beta^B \exp(-A\beta)$, the values being $B = 3$ in the infinite L limit and $B = 2$ in the finite L limit with $A = 4$ in both limits. We show in Fig. 26 FF specific heat data for a wide range of sizes in the form $y(\beta, L) = \partial \ln C_v(\beta, L)/\partial\beta$ against $x = T$. This type of plot leads to a straight line with intercept $-A$ and slope B. For finite sizes in the FF model there is a crossover at a size dependent temperature $T^*(L)$, just as in the 2D bimodal ISG [10, 41]. The FF $T^*(L)$ crossover from an effectively continuous energy level regime to the ground state plus gap dominated regime can be identified by inspection of Fig. 26 as the region where for each L the curve $y(x)$ passes from the thermodynamic limit $T > T^*(L)$ envelope curve $y(x) \approx -4 + 3.5x$ to the finite size ground state dominated regime $T < T^*(L)$ line $y(x) = -4 + 2x$. The A and B values practically agree with Ref. [31]; the crossover temperatures are near $T^*(L) \approx 0.5$. The present figure can be compared directly to the equivalent figure for the 2D bimodal ISG, Ref. [1] Fig. 2. The lower diagonal line in the present Fig. 26 corresponds to just the same "naïve" ground state plus $4J$ gap dominated specific heat regime as in the 2D bimodal ISG, $C_v(T) \sim \exp(-4/T)/T^2$, but the 2D bimodal ISG large L thermodynamic limit specific heat curve with $A \approx 0$ and B negative is very different from the FF large L limit curve.

The FF $U_4(\beta, L)$ against $\xi(\beta, L)/L$ curve breaks off rapidly from the $\eta = 0$ universal curve to arrive smoothly at a critical end-point $\xi(T = 0, L)/L = 0.488 + 0.1/L$, $U_4(T = 0, L) = 1.618 - 0.2/L$) [27], Fig. 27.

In Fig. 28, we show the FF derivative $y(\beta, L) = \partial \ln \chi(\beta, L)/\partial \ln \xi(\beta, L)$ against $x(\beta, L) = 1/\xi(\beta, L)$, where $\xi(\beta, L)$ is the second moment correlation length and $\chi(\beta, L)$ is the susceptibility. In the present Fig. 28 (as in the bimodal and Gaussian ISG figures in Ref. [1], Figs. 3 and 4) for all the ThL envelope points the data are in the regime $T > T^*(L)$.

The L-independent envelope curve of all the FF data in the ThL regime $L > \xi(\beta, L)$, $T > T^*(L)$ can be identified by inspection. The essential point is that the "high temperature" regime FF ThL derivative $y(\beta, L)$ from temperatures above the crossovers extrapolates smoothly and accurately to $y(\beta, L) = 1.5$, so to $y(\beta, L) = 2 - \eta$ with an effective limiting η equal to 1/2, the analytically known $L = \infty$, $T = 0$ critical exponent [39].

Thus in the FF model, it is found that when the "effectively continuous energy level" regime effective exponent $\eta(T, L)$ is extrapolated to the limit of large L using the ThL $\partial \ln \chi(\beta, L)/\partial \ln \xi(\beta, L)$ differentiation procedure, the value is equal to the $T \equiv 0$ ground state critical exponent. This can be taken to imply that there is no difference between these two limiting exponent values in the discrete interaction distribution ISG models either.

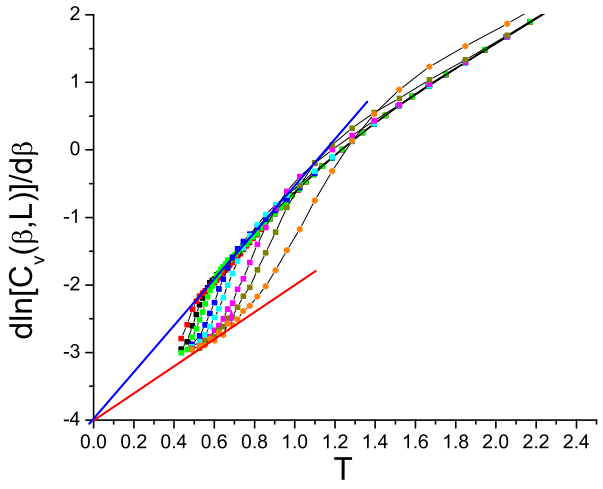

FIG. 26. (Color on line) Fully Frustrated 2D model. The logarithmic derivative of the specific heat $\partial \ln C_v(\beta, L)/\partial \ln \beta$ against temperature T. $L = 96, 64, 48, 32, 24, 16, 12, 8$ (left to right). Upper blue straight line : the thermodynamic limit $T > T^*(L)$ envelope curve $y(x) = -4 + 3.5x$. Lower red straight line : the finite size ground state dominated $T < T^*(L)$ regime $y(x) = -4 + 2x$.

Appendix B: Fitting procedure

In Ref. [1] the data for the derivative of the susceptibility and the second moment correlation length $\gamma_b(\tau_b, L) = \partial \ln \chi(\beta, L)/\partial \ln \tau_b$ and $\nu_b(\tau_b, L) = \partial \ln[\xi(\beta, L)/\beta]/\partial \ln \tau_b$ were extrapolated to $\tau_b = 0$ after making three parameter polynomial fits of the type $y(\tau_b) = a + b\tau_b + c\tau_b^2$.

In the present work we carry out the same type of fit but in two stages. First we plot the higher derivatives $\partial\gamma_b(\tau_b, L)/\partial\tau_b$ and $\partial\nu_b(\tau_b, L)/\partial\tau_b$ against τ_b. In each case a two parameter straight line fit $y(\tau_b) = b + 2c\tau_b$ to the ThL data up to about $\tau_b = 0.50$ is quite acceptable. This implies that the leading Wegner correction exponent θ happens to be close to 1.0 in all models, as was assumed in Ref. [1], and justifies the simple polynomial fit procedure. Susceptibility $\partial\gamma_b(\tau_b, L)/\partial\tau_b$ data are shown in Figs. 29, 30, 31, 32, and 33. The $\partial\nu_b(\tau_b, L)/\partial\tau_b$ data have a similar aspect but are intrinsically more noisy. With the parameters b and c in hand for each model and so with a single remaining free parameter, a, fits were made up to $\tau_b \approx 0.50$ to each of the $\gamma_b(\tau_b, L)$ and $\nu_b(\tau_b, L)$ ThL curves shown in the earlier sections.

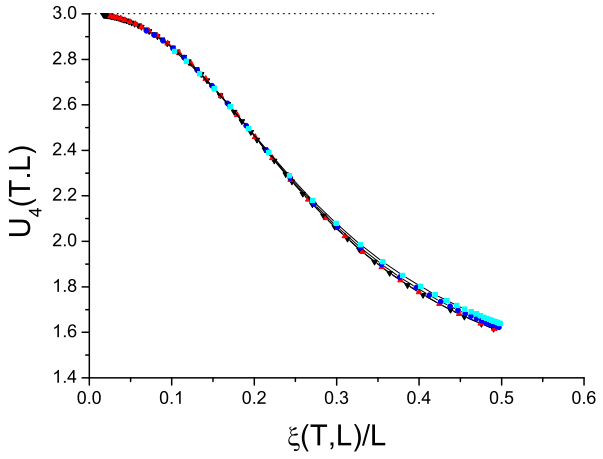

FIG. 27. (Color on line) Fully Frustrated 2D model. The low temperature Binder cumulant $U_4(T, L)$ against the normalized correlation length $\xi(T, L)/L$. $L = 8$ (cyan squares), $L = 12$ (blue circles), $L = 32$ (red triangles), $L = 48$ (black inverted triangles). For each L the data points terminate smoothly at a zero temperature end-point.

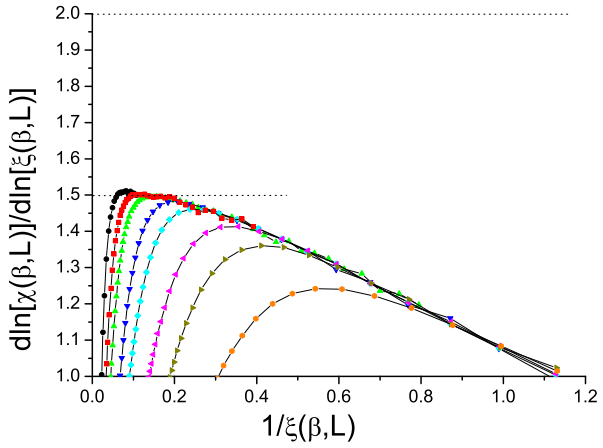

FIG. 28. (Color on line) Fully Frustrated 2D model. The logarithmic derivative $\partial \ln \chi(\beta, L)/\partial \ln \xi(\beta, L)$ against $1/\xi(\beta, L)$. $L = 96$, 64, 48, 32, 24, 16, 12, 8 (left to right).

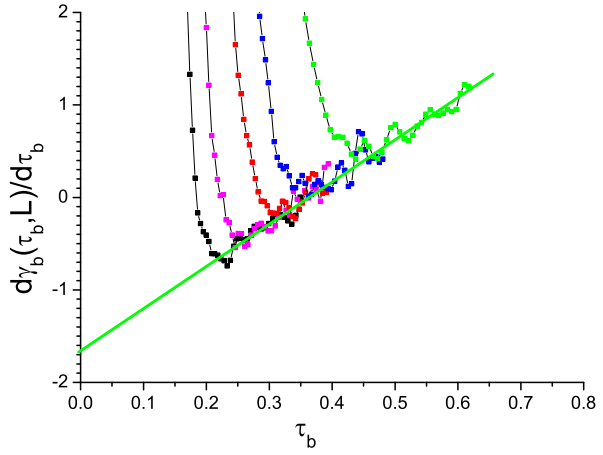

FIG. 29. (Color on line) Gaussian 2D ISG. The derivative $\partial\gamma_b(\tau_b, L)/\partial\tau_b$ against τ_b for $L = 128$, 96, 64, 48, 32 (left to right). Straight green line : fit to the ThL regime data

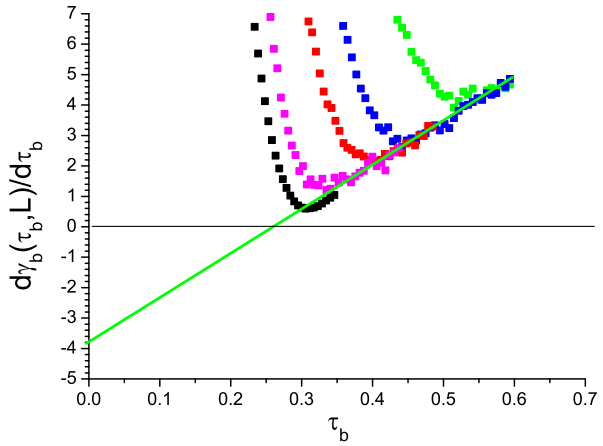

FIG. 30. (Color on line) Bimodal 2D ISG. The derivative $\partial\gamma_b(\tau_b, L)/\partial\tau_b$ against τ_b for $L = 128$, 96, 64, 48, 32 (left to right). Straight green line : fit to the ThL regime data

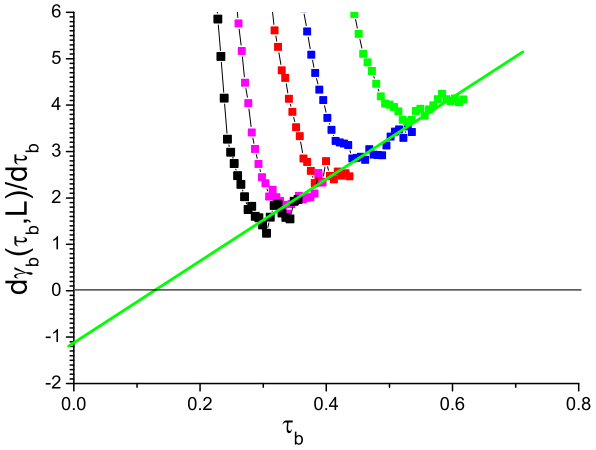

FIG. 31. (Color on line) Diluted bimodal 2D ISG. The derivative $\partial\gamma_b(\tau_b, L)/\partial\tau_b$ against τ_b for $L = 128$, 96, 64, 48, 32 (left to right). Straight green line : fit to the ThL regime data

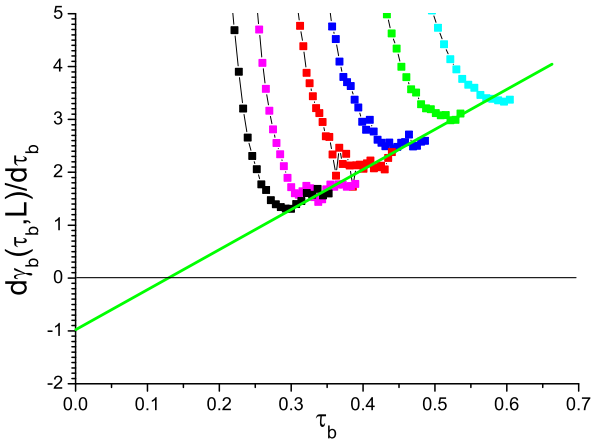

FIG. 32. (Color on line) Anti-diluted bimodal 2D ISG. The derivative $\partial\gamma_b(\tau_b, L)/\partial\tau_b$ against τ_b for $L = 128$, 96, 64, 48, 32, 24 (left to right). Straight green line : fit to the ThL regime data

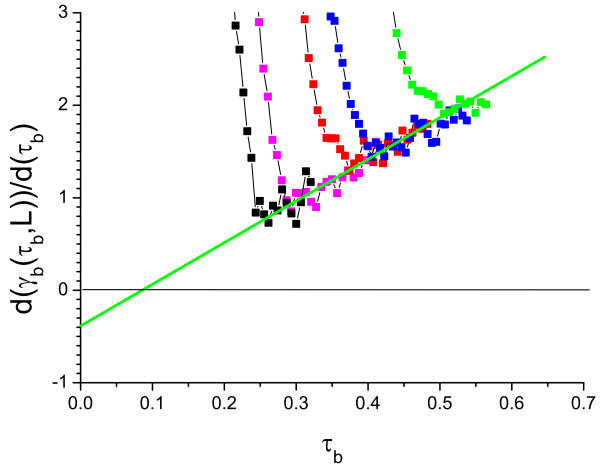

FIG. 33. (Color on line) Symmetric Poisson 2D ISG. The derivative $\partial\gamma_b(\tau_b, L)/\partial\tau_b$ against τ_b for $L = 128$, 96, 64, 48, 32 (left to right). Straight green line : fit to the ThL regime data